General Disclaimer

One or more of the Following Statements may affect this Document

- This document has been reproduced from the best copy furnished by the organizational source. It is being released in the interest of making available as much information as possible.

- This document may contain data, which exceeds the sheet parameters. It was furnished in this condition by the organizational source and is the best copy available.

- This document may contain tone-on-tone or color graphs, charts and/or pictures, which have been reproduced in black and white.

- This document is paginated as submitted by the original source.

- Portions of this document are not fully legible due to the historical nature of some of the material. However, it is the best reproduction available from the original submission.

BIMONTHLY REPORT

(NASA-CR-150486) DIGITAL CONTROLLER DESIGN: ANALYSIS OF THE ANNULAR SUSPENSION POINTING SYSTEM Bimonthly Report (Systems Research Lab., Champaign, Ill.) 34 p HC A03/MF A01 CSCL 22B G3/16

N78-14090

Unclas 59478

RESEARCH STUDY ON STABILIZATION AND CONTROL

MODERN SAMPLED-DATA CONTROL THEORY

SYSTEMS RESEARCH LABORATORY

P.O. BOX 2277, STATION A
3206 VALLEY BROOK DRIVE
CHAMPAIGN, ILLINOIS 61820

PREPARED FOR GEORGE C. MARSHALL SPACE FLIGHT CENTER

HUNTSVILLE, ALABAMA

BIMONTHLY REPORT

DIGITAL CONTROLLER DESIGN

subtitle:

ANALYSIS OF THE ANNULAR SUSPENSION

POINTING SYSTEM

December 1, 1977

Contract No. NAS8-32358 1-7-ED-07418(IF)

PREPARED FOR GEORGE C. MARSHALL SPACE FLIGHT CENTER

HUNTSVILLE, ALABAMA

SYSTEMS RESEARCH LABORATORY

P.O. BOX 2277, STATION A

CHAMPAIGN, ILLINOIS 61820

VII. SIMPLIFIED MODELS OF THE ANNULAR SUSPENSION AND POINTING SYSTEM (ASPS)

7.1 Introduction [1]

The Annular Suspension and Pointing System (ASPS) is a payload auxiliary pointing device of the Space Shuttle. The ASPS is comprised of two major subassemblies, a vernier and a coarse pointing subsystem.

The experiment is attached to a mounting plate/rim combination which is suspended on magnetic bearing/actuators (MBA's) strategically located about the rim. Fine pointing is achieved by "gimballing" the plate/rim within the MBA gaps. Control about the experiment line-of-sight is obtained through the use of a non-contacting rim drive and positioning torquer. All sensors used to close the servo loops on the vernier system are noncontacting elements. Therefore, the experiment is a free-flyer constrained only by the magnetic forces generated by the control loops.

The configuration of the ASPS is shown in Fig. 7-1. The payload/plate/rim combination is mounted on a set of coarse gimbals; an elevation and a lateral coarse gimbal, which provide the slewing and coarse pointing capability of the system. The pointing system concept is unique in that the vernier and coarse pointing subsystem are separate entities. This approach allows for sub-arcsecond pointing of the payload at any coarse gimbal position.

The three functions provided by the ASPS are: (1) pointing the payload, (2) centering the payload in the magnetic actuator assembly, and (3) tracking the payload mounting plate and shuttle motions by the coarse gimbals. Rate and position errors sensed by gyros and celestial sensors located on the payload are processed by a controller which subsequently commands appropriate actuator forces to point the payload. Proximeter sensors associated with the actuator clusters detect the payload translation errors which are subsequently processed by the

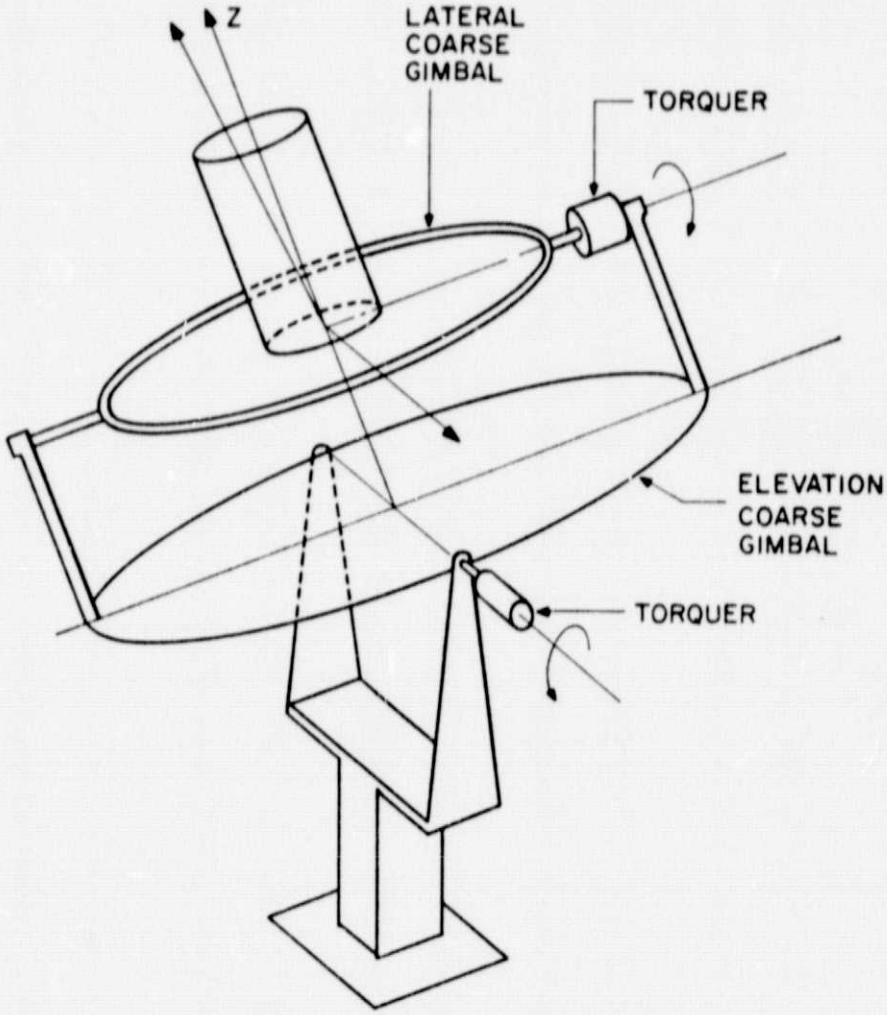

Figure 7-1. ASPS configuration.

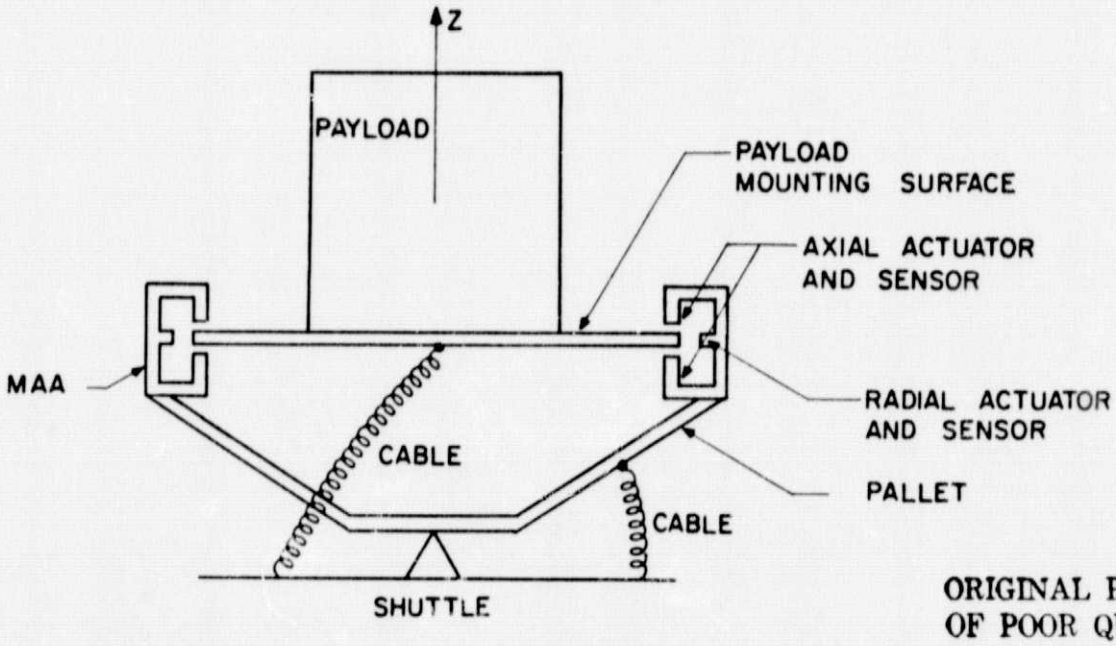

Figure 7-2. Payload and magnetic actuator assembly.

controller and used to ascertain the appropriate centering forces.

Figure 7-2 shows the payload and its mounting surface which is controlled by the magnetic actuator assembly (MAA). The cables shown are for the purpose of connecting electric power from the shuttle to the payload and the MAA on the pallet.

7.2 The Planar Model of the ASPS [2]

In this section the equations of motion of a simplified planar model of the ASPS are derived.

The small-angle, small-displacement model shown in Fig. 7-3 is planar with four degrees of freedom and is composed of a mount, a gimbal assembly (elevation), a pallet with magnetic actuators, and a payload. The pallet has one rotational degree of freedom relative to the mount, and the payload has two translational and one rotational degrees of freedom relative to the pallet.

Let the four degrees of freedom be

ϕ_1 = attitude degree of freedom of the pallet relative to the mount

ϕ_2 = attitude degree of freedom of the payload relative to the pallet

x_1 = translation degree of freedom of the payload relative to the pallet

z_1 = translation degree of freedom of the payload relative to the pallet

The following coordinates are defined:

(x_0, z_0) = inertial axes

(x_G, z_G) = inertial axes rotated through an angle of ϕ_M relative to the (x_0, z_0) axes, (ϕ_M is defined as the gimbal angle).

(x_m, z_m) = axes fixed at the pallet center of gravity (CG)

(x_1, z_1) = static axes of the payload

(x_i, z_i) = axes fixed at the payload center of gravity (CG)

(x_j, z_j) = axes fixed at the center of the base of the payload.

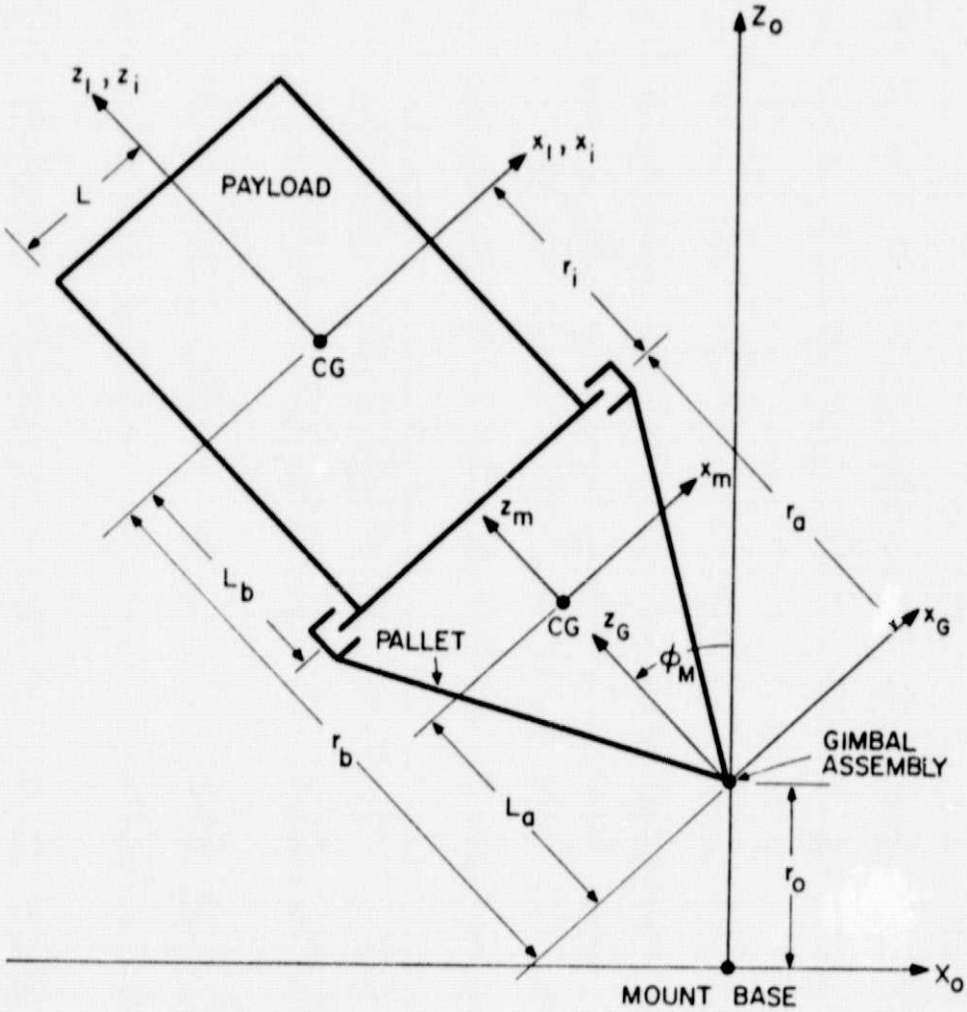

Figure 7-3. Planar ASPS model.

The following system parameters are defined:

M_i = mass of the payload = 600 Kg

M_m = mass of the pallet = 82 Kg

J_m = inertia of the pallet about its mass center = 3.1 Kg-m^2

J_i = inertia of the payload about its mass center = 503 Kg-m^2

L = radius of the payload = 0.406 m

L_a = distance from the gimbal to the pallet CG = 0.2064 m

L_b = distance from the pallet center to the payload CG = 1.486 m

r_a = distance from the gimbal assembly to the pallet center = 0.47 m

r_b = distance from the gimbal assembly to the payload CG = 1.956 m

r_0 = distance from the mount base to the gimbal assembly = 0.75 m

Since the payload is suspended with respect to the pallet, there are many ways of fixing its coordinates for the motion of rotation. In other words, the angle ϕ_2 can be defined in a number of ways. Figure 7-4 illustrates the small-angle rotation of the pallet and the payload with ϕ_2 measured as the angle between the coordinate axes of (x_1,z_1) and (x_j,z_j). This configuration is defined as Model 1 of the ASPS. Figure 7-5 illustrates the model of the ASPS with ϕ_2 measured at the CG of the payload; i.e., between the axes of (x_1,z_1) and (x_i,z_i).

The following coordinate transformations are identified:

Transformation from the static pallet axes to the mount axes:

$$T_G = \begin{bmatrix} \cos\phi_M & -\sin\phi_M \\ \sin\phi_M & \cos\phi_M \end{bmatrix} \tag{7-1}$$

Transformation from the dynamic pallet axes to the static pallet axis:

$$T_1 = \begin{bmatrix} \cos\phi_1 & -\sin\phi_1 \\ \sin\phi_1 & \cos\phi_1 \end{bmatrix} \cong \begin{bmatrix} 1 & -\phi_1 \\ \phi_1 & 1 \end{bmatrix} \tag{7-2}$$

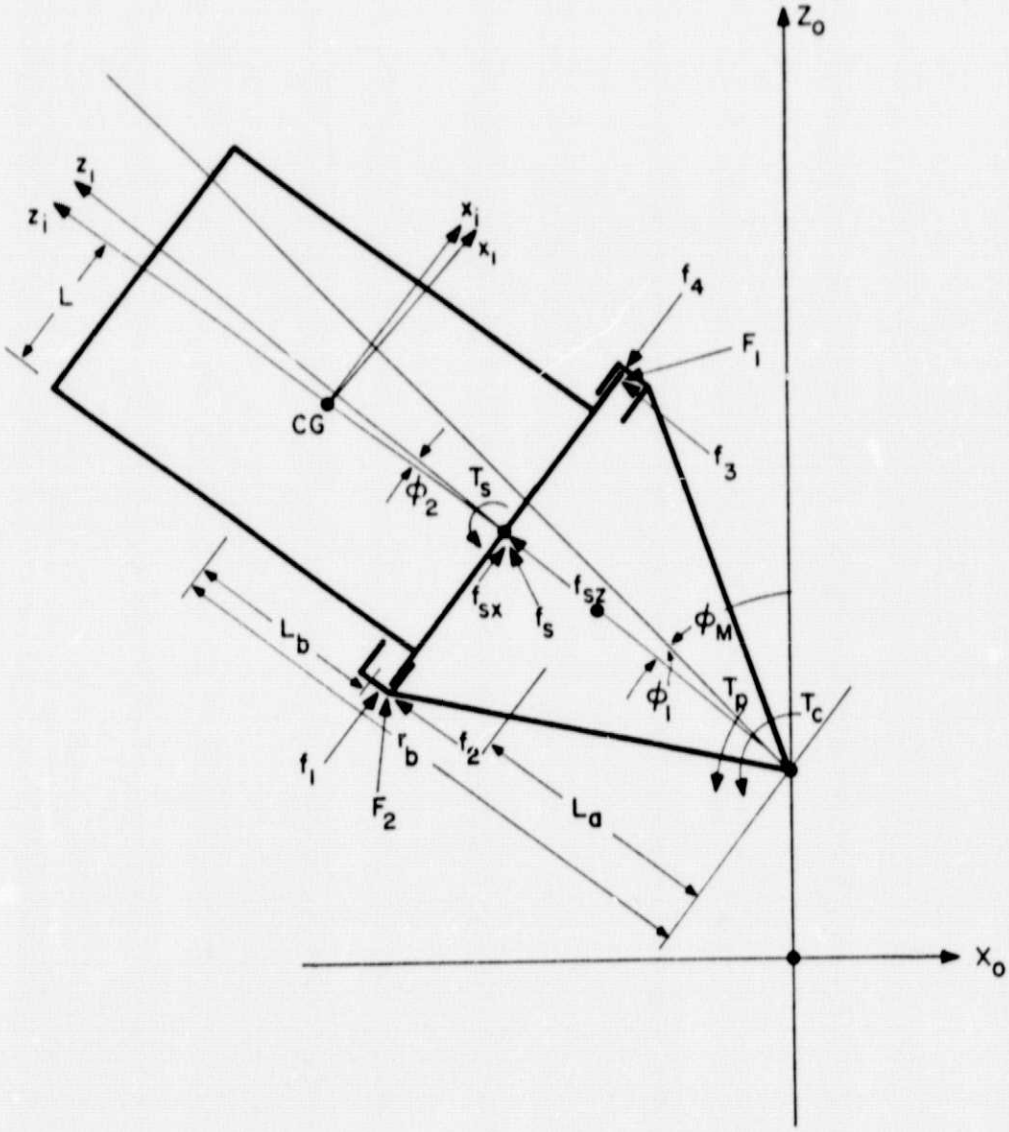

Figure 7-4. Planar ASPS Model 1.

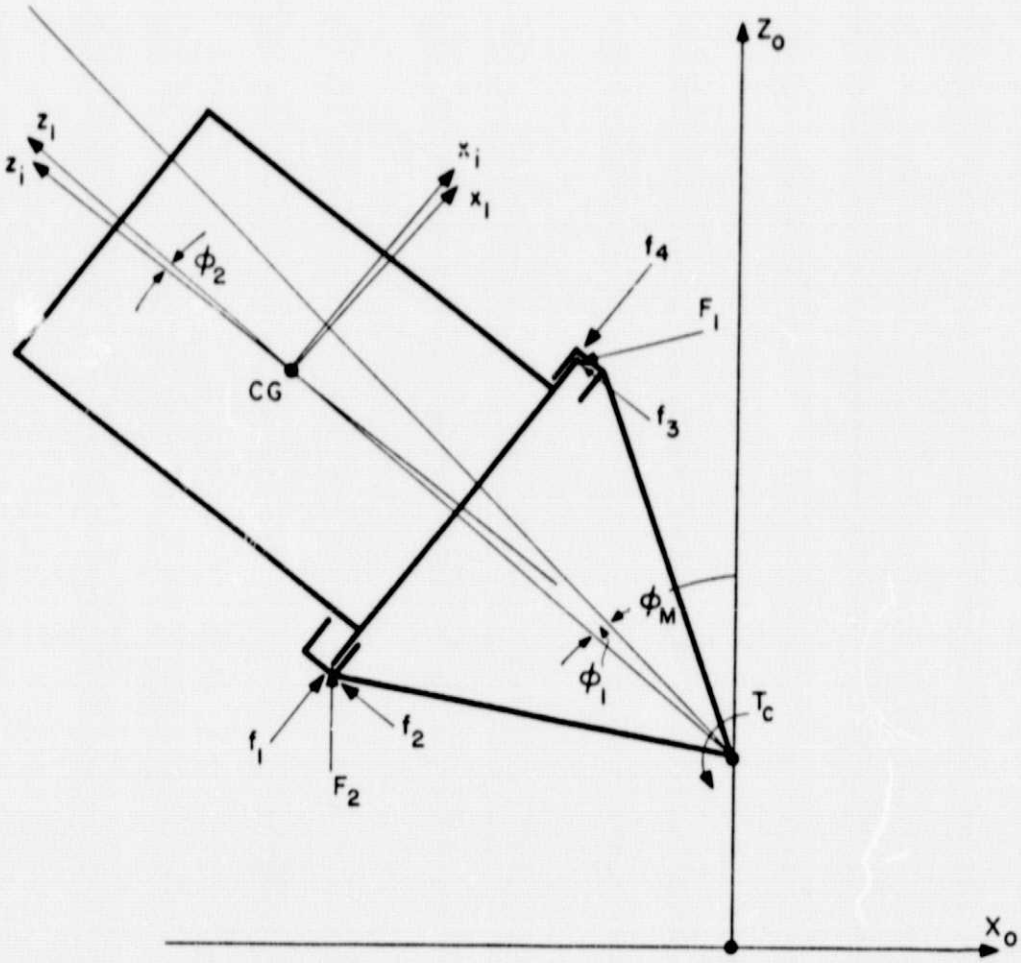

Figure 7-5. Planar ASPS Model 2.

Transformation from the dynamic payload axes to the dynamic pallet axes:

$$T_2 = \begin{bmatrix} \cos\phi_2 & -\sin\phi_2 \\ \sin\phi_2 & \cos\phi_2 \end{bmatrix} = \begin{bmatrix} 1 & -\phi_2 \\ \phi_2 & 1 \end{bmatrix} \tag{7-3}$$

The force vectors applied to the payload by the magnetic actuator assembly are defined as:

$$F_1 = \begin{bmatrix} f_4 \\ f_3 \end{bmatrix} = \text{magnetic force applied at the positive } x_m \text{ displacement} \tag{7-4}$$

$$F_2 = \begin{bmatrix} f_1 \\ f_2 \end{bmatrix} = \text{magnetic force applied at the negative } x_m \text{ displacement} \tag{7-5}$$

The forces F_1 and F_2 are illustrated as shown in Fig. 7-5.

The torque applied by the gimbal assembly is designated as T_c, as shown in Fig. 7-5.

The following vector distances are defined for the pallet and the payload.

R_1 = vector distance from the gimbal assembly to the payload point of application of F_1

R_2 = vector distance from the gimbal assembly to the payload point of application of F_2

R_3 = vector distance from the gimbal assembly to the pallet point of application of F_1

R_4 = vector distance from the gimbal assembly to the pallet point of application of F_2.

Equations of Motion of Model 1

Using the degrees of freedom defined in the preceding sections, the kinetic energy of the system in Fig. 7-4 is

$$T = K.E. = \frac{1}{2}\dot{R}_m' M_m \dot{R}_m + \frac{1}{2}\dot{R}_i' M_i \dot{R}_i + \frac{1}{2}J_m \dot{\phi}_1^2 + \frac{1}{2}J_i(\dot{\phi}_1 + \dot{\phi}_2)^2 \tag{7-6}$$

where the primes denote the transpose of a matrix, and

$$\dot{R}_m = \begin{bmatrix} -L_a \\ 0 \end{bmatrix} \dot{\phi}_1 \tag{7-7}$$

$$\dot{R}_i = \begin{bmatrix} \dot{x}_1 \\ \dot{z}_1 \end{bmatrix} + \begin{bmatrix} -L_b \\ 0 \end{bmatrix} \dot{\phi}_2 + \begin{bmatrix} -r_b \\ 0 \end{bmatrix} \dot{\phi}_1 \tag{7-8}$$

Substitution of Eqs. (7-7) and (7-8) into Eq. (7-6) gives

$$T = K.E. = \frac{1}{2}M_m L_a^2 \dot{\phi}_1^2 + \frac{1}{2}M_i \dot{z}_1^2 + \frac{1}{2}M_i(\dot{x}_1 - r_b\dot{\phi}_1 - L_b\dot{\phi}_2)^2 + \frac{1}{2}J_m\dot{\phi}_1^2 + \frac{1}{2}J_i(\dot{\phi}_1 + \dot{\phi}_2)^2 \tag{7-9}$$

Let the spring force applied to the system payload due to the cable be designated as

$$f_s = \begin{bmatrix} f_{sx}(x_1) \\ f_{sz}(z_1) \end{bmatrix} \tag{7-10}$$

and the spring torque applied to the payload due to the cable be $T_s(\phi_2)$. The spring torque applied to the pallet due to the cable is denoted as $T_p(\phi_1)$.

The relation between the force $\overline{F}$ and the potential of the system, U, is

$$\overline{F} = -\nabla U \tag{7-11}$$

Thus,

$$U = U_0 - \int \overline{F} \cdot d\overline{x} \tag{7-12}$$

where U_0 = constant.

The potential energy of Model 1 is

$$U = U_0 - \{(f_1 - f_4)x_1 + (f_2 + F_3)z_1 + \int_0^{\phi_2} T_s(\phi)d\phi + \int_0^{z_1} f_{sz}(z)dz + \int_0^{x_1} f_{sx}(x)dx$$

$$+ (f_3 - f_2)L\phi_2 + \int_0^{\phi_1} T_c(\phi)d\phi + \int_0^{\phi_1} T_p(\phi)d\phi \tag{7-13}$$

The Lagrangian is defined as

$$\mathcal{L} = K.E. - U \tag{7-14}$$

Then from Eqs. (7-9) and (7-13), we get

$$\mathcal{L} = \frac{1}{2}M_m L_a^2\dot{\phi}_1^2 + \frac{1}{2}M_i\dot{z}_1^2 + \frac{1}{2}M_i(\dot{x}_1 - r_b\dot{\phi}_1 - L_b\dot{\phi}_2)^2 + \frac{1}{2}J_m\dot{\phi}_1^2 + \frac{1}{2}J_i(\dot{\phi}_1 + \dot{\phi}_2)^2$$

$$+ (f_1 - f_4)x_1 + (f_2 + f_3)z_1 + \int_0^{\phi_2} T_s(\phi)d\phi + \int_0^{z_1} f_{sz}(z)dz + \int_0^{x_1} f_{sx}(x)dx$$

$$+ (f_3 - f_2)L\phi_2 + \int_0^{\phi_1} T_c(\phi)d\phi + \int_0^{\phi_1} T_p(\phi)d\phi - U_0 \qquad (7\text{-}15)$$

The Lagrange equation of motion is

$$\frac{\partial\mathcal{L}}{\partial x_i} - \frac{d}{dt}\left(\frac{\partial}{\partial\dot{x}_i}\right) = 0 \qquad i = 1,2,3,4 \qquad (7\text{-}16)$$

where $x_1 = x_1$, $x_2 = z_1$, $x_3 = \phi_1$ and $x_4 = \phi_2$.

For i = 1, we have

$$\frac{\partial\mathcal{L}}{\partial x_1} = f_1 - f_4 + f_{sx}(x_1) \qquad (7\text{-}17)$$

$$\frac{\partial\mathcal{L}}{\partial\dot{x}_1} = M_i(\dot{x}_1 - r_b\dot{\phi}_1 - L_b\dot{\phi}_2)$$

Thus,

$$\frac{\partial\mathcal{L}}{\partial x_1} - \frac{d}{dt}\left(\frac{\partial}{\partial\dot{x}_i}\right) = -M_i\ddot{x}_1 + M_i r_b\ddot{\phi}_1 + M_i L_b\ddot{\phi}_2 + (f_1 - f_4) + f_{sx}(x_1) = 0 \qquad (7\text{-}18)$$

For i = 2, we have

$$\frac{\partial\mathcal{L}}{\partial z_1} = f_2 + f_3 + f_{sz}(z_1)$$

$$\frac{\partial\mathcal{L}}{\partial\dot{z}_1} = M_i\dot{z}_i$$

Then,

$$\frac{\partial\mathcal{L}}{\partial z_1} - \frac{d}{dt}\left(\frac{\partial}{\partial\dot{z}_1}\right) = -M_i\ddot{z}_i + (f_2 + f_3) + f_{sz}(z_1) = 0 \qquad (7\text{-}19)$$

For i = 3, we have

$$\frac{\partial\mathcal{L}}{\partial\phi_1} = T_c(\phi_1) + T_p(\phi_1)$$

$$\frac{\partial\mathcal{L}}{\partial\dot{\phi}_1} = M_m L_{az}^2\dot{\phi}_1 + M_i(-r_b\dot{x}_1 + r_b^2\dot{\phi}_1 + r_b L_b\dot{\phi}_2) + J_m\dot{\phi}_1 + J_i\dot{\phi}_1 + J_i\dot{\phi}_2$$

$$\frac{\partial}{\partial\phi_1} - \frac{d}{dt}\left(\frac{\partial\mathcal{L}}{\partial\dot{\phi}_1}\right) = T_c(\phi_1) + T_p(\phi_1) + M_i r_b \ddot{x}_1$$

$$- (J_m + J_i + M_m L_a^2 + M_i r_b^2)\ddot{\phi}_1 - (J_i + M_i L_b r_b)\ddot{\phi}_2 = 0 \quad (7\text{-}20)$$

For i = 4, we have

$$\frac{\partial\mathcal{L}}{\partial\phi_2} = (f_3 - f_2)L + T_s(\phi_2)$$

$$\frac{\partial\mathcal{L}}{\partial\dot{\phi}_2} = -M_i L_b \dot{x}_1 + r_b L_b M_i \dot{\phi}_1 + M_i L_b^2 \dot{\phi}_2 + J_i \dot{\phi}_1 + J_i \dot{\phi}_2$$

$$\frac{\partial\mathcal{L}}{\partial\phi_2} - \frac{d}{dt}\left(\frac{\partial}{\partial\dot{\phi}_2}\right) = T_s(\phi_2) + (f_3 - f_2)L + M_i L_b \ddot{x}_1$$

$$- (M_i L_b r_b + J_i)\ddot{\phi}_1 - (M_i L_b^2 + J_i)\ddot{\phi}_2 = 0 \quad (7\text{-}21)$$

The Lagrange equations in Eqs. (7-18), (7-19), (7-20) and (7-21) are written in matrix form as follows:

$$\begin{bmatrix} M_i & 0 & -M_i r_b & -M_i L_b \\ 0 & M_i & 0 & 0 \\ -M_i r_b & 0 & J_m+J_i+M_m L_a^2+M_i r_b^2 & J_i+M_i L_b r_b \\ -M_i L_b & 0 & J_i+M_i L_b r_b & J_i+M_i L_b^2 \end{bmatrix} \begin{bmatrix} \ddot{x}_1 \\ \ddot{z}_1 \\ \ddot{\phi}_1 \\ \ddot{\phi}_2 \end{bmatrix} = \begin{bmatrix} f_1-f_4+f_{sx}(x_1) \\ f_2+f_3+f_{sx}(z_1) \\ T_c(\phi_1)+T_p(\phi_1) \\ (f_3-f_2)L+T_s(\phi_2) \end{bmatrix} \quad (7\text{-}22)$$

Equations of Motion of Model 2

For the ASPS system Model 2, the kinetic energy of the system is still given by Eq. (7-6), and $\dot{R}_m$ is as defined in Eq. (7-7), except that

$$\dot{R}_i = \begin{bmatrix} \dot{x}_1 \\ \dot{z}_1 \end{bmatrix} + \begin{bmatrix} -r_b \\ 0 \end{bmatrix} \dot{\phi}_1 \quad (7\text{-}23)$$

Substitution of Eqs. (7-7) and (7-23) into Eq. (7-6) gives

$$K.E. = \frac{1}{2}M_m L_a^2 \dot{\phi}_1^2 + \frac{1}{2}M_i \dot{z}_1^2 + \frac{1}{2}M_i(\dot{x}_1 - r_b\dot{\phi}_1)^2 + \frac{1}{2}J_m\dot{\phi}_1^2 + \frac{1}{2}J_i(\dot{\phi}_1 + \dot{\phi}_2)^2 \quad (7\text{-}24)$$

The potential energy of the Model 2 is

$$U = U_0 - \{(f_1 - f_4)x_1 + \int_0^{x_1} f_{sx}(x)dx + (f_2 + f_3)z_1 + \int_0^{z_1} f_{sz}(z)dz + \int_0^{\phi_2} T_s(\phi)d\phi$$

$$+ \int_0^{\phi_1} T_c(\phi)d\phi + \int_0^{\phi_1} T_p(\phi)d\phi + (f_3 - f_2)L\phi_2 + (f_1 - f_4)L_b\phi_2\} \qquad (7\text{-}25)$$

The Lagrangian $\mathcal{L}$ is given by

$$\mathcal{L} = \text{K.E.} - U = \frac{1}{2}M_m L_a^2\dot{\phi}_1^2 + \frac{1}{2}M_i\dot{z}_1^2 + \frac{1}{2}M_i(\dot{x}_1 - r_b\dot{\phi}_1)^2 + \frac{1}{2}J_m\dot{\phi}_1^2 + \frac{1}{2}J_i(\dot{\phi}_1 + \dot{\phi}_2)^2$$

$$+ (f_1 - f_4)x_1 + \int_0^{x_1} f_{sx}(x)dx + (f_2 + f_3)z_1 + \int_0^{z_1} f_{sz}(z)dz$$

$$+ \int_0^{\phi_2} T_s(\phi)d\phi + \int_0^{\phi_1} T_c(\phi)d\phi + \int_0^{\phi_1} T_p(\phi)d\phi + \{(f_3 - f_2)L$$

$$+ (f_1 - f_4)L_b\}\phi_2 - U_0 \qquad (7\text{-}26)$$

The Lagrange equation of motion is given by Eq. (7-16).

Following the same procedure as for Model 1, the Lagrange equations of Model 2 are derived by use of Eqs. (7-16) and (7-26), and the result is

$$\begin{bmatrix} M_i & 0 & -M_i r_b & 0 \\ 0 & M_i & 0 & 0 \\ -M_i r_b & 0 & J_m + J_i + M_m L_a^2 + M_i r_b^2 & J_i \\ 0 & 0 & J_i & J_i \end{bmatrix} \begin{bmatrix} \ddot{x}_1 \\ \ddot{z}_1 \\ \ddot{\phi}_1 \\ \ddot{\phi}_2 \end{bmatrix} = \begin{bmatrix} f_1 - f_4 + f_{sx}(x_1) \\ f_2 + f_3 + f_{sz}(z_1) \\ T_c(\phi_1) + T_p(\phi_1) \\ (f_3 - f_2)L + (f_1 - f_4)L_b + T_s(\phi_2) \end{bmatrix}$$

(7-27)

In the analysis conducted in the ensuing sections the equations of motions of Model 2 will be used. One reason for this selection is that the mass matrix of Eq. (7-27) is simpler than that of Model 1 in Eq. (7-22). Another reason for using Model 2 is that the model uses the center of gravity of the payload as the reference point of rotation, which is more logical.

Substitution of the system parameters into Eq. (7-27), we have

$$\begin{bmatrix} 600 & 0 & -1173.6 & 0 \\ 0 & 600 & 0 & 0 \\ -1173.6 & 0 & 2805.15 & 503 \\ 0 & 0 & 503 & 503 \end{bmatrix} \begin{bmatrix} \ddot{x}_1 \\ \ddot{z}_1 \\ \ddot{\phi}_1 \\ \ddot{\phi}_2 \end{bmatrix} = \begin{bmatrix} f_1 - f_4 + f_{sx}(x_1) \\ f_2 + f_3 + f_{sz}(z_1) \\ T_c(\phi_1) + T_p(\phi_1) \\ (f_3 - f_2 L + (f_1 - f_4) L_b + T_s(\phi_2) \end{bmatrix} \tag{7-28}$$

7.3 Control of the Z_1 Dynamics of the Payload

Equation (7-28) indicates that the z_1 dynamics of the ASPS are not coupled to the other three degrees of freedom. The z_1 dynamics are described by

$$M_i \ddot{z}_1 = f_2 + f_3 + f_{sz}(z_1) \tag{7-29}$$

The magnetic actuator forces $f_2 + f_3$ are controlled by feeding back the variables z_1 and $\dot{z}_1$. The control equation is

$$f_2 + f_3 = -K_p z_1 - K_r \dot{z}_1 \tag{7-30}$$

where $K_p = 37.861$ N/m and $K_r = 211.01$ N/m/sec.

Substitution of Eq. (7-30) into Eq. (7-29), we have

$$M_i \ddot{z}_1 = -K_p z_1 - K_r \dot{z}_1 + f_{sz}(z_1) \tag{7-31}$$

Figure 7-6 shows the state diagram of the z_1 dynamics of the ASPS with the continuous-data position-plus-rate controller. The notation $N_{sz}(z_1)$ in the state diagram represents the functional relation of the wire cable which is attached to the center of the payload mounting surface.

If the wire cable is modelling by a linear spring, $N_{sz}(z_1)$ is simply a constant, $-K_s$ (N/m); that is,

$$f_{sz}(z_1) = -K_s z_1 \tag{7-32}$$

A nonlinear spring characteristic for $N_{sz}(z_1)$ is shown in Fig. 7-7. However, since the mass of the payload is 600 Kg, and the spring constant is

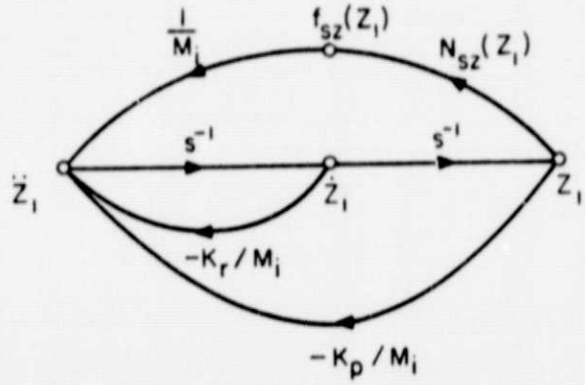

Figure 7-6. State diagram of the z_1 dynamics of the ASPS with position-plus-rate controller (continuous-data system).

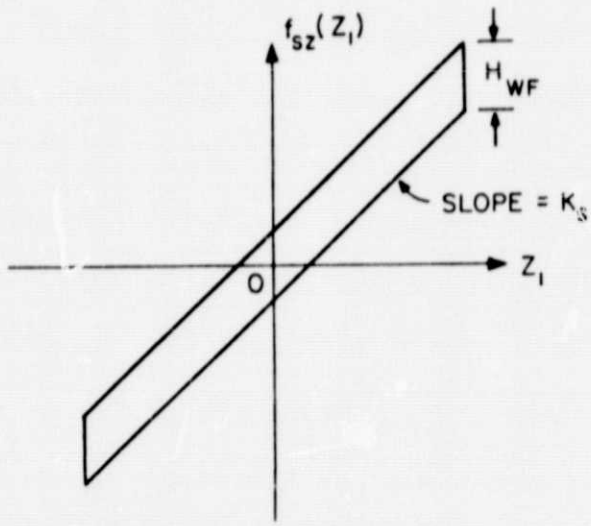

Figure 7-7. Nonlinear spring characteristic for the wire-cable torque of the ASPS.

only 0.35 N/m, the effect of the wire cable on the payload dynamics is not going to be substantial.

The characteristic equation of the continuous-data ASPS z_1 dynamic system with the linear wire cable spring characteristic is

$$M_i s^2 + K_r s + K_p + K_s = 0 \tag{7-33}$$

or

$$600s^2 + 211.01s + 38.211 = 0 \tag{7-34}$$

The damping ratio of the system is

$$\zeta = 0.6968 \tag{7-35}$$

and the undamped natural frequency is

$$\omega_n = 0.2524 \text{ rad/sec} \tag{7-36}$$

Analysis of the Digital ASPS z_1 Dynamics

When the z_1 dynamics of the ASPS are controlled by a digital position-plus-rate controller, the dynamic equation is

$$M_i \ddot{z}_1 + K_s z_1 = f_2(t) + f_3(t) \tag{7-37}$$

where

$$f_2(t) + f_3(t) = f_2(kT) + f_3(kT) \qquad kT \leq t < (k+1)T \tag{7-38}$$

Then the control equation is

$$f_2(kT) + f_3(kt) = -K_p z_i(kT) - K_r \dot{z}_i(kT) \tag{7-39}$$

Figure 7-8 shows the block diagram of the linear digital ASPS payload (z_1 dynamics).

Since all the system parameters are given, except the sampling period T, we shall study the maximum value of T for asymptotic stability.

The characteristic equation of the digital system in Fig. 7-8 is

$$\Delta(z) = 1 + \frac{1}{M_i}(1 - z^{-1})\mathcal{Z}\left\{\frac{K_r/s^2}{1 + \frac{K_r}{M_i} s^{-2}} + \frac{K_p/s^3}{1 + \frac{K_s}{M_i} s^{-2}}\right\} = 0 \tag{7-40}$$

The z-transforms in the last equation are evaluated as follows:

$$\mathcal{Z}\left(\frac{1}{s^2 + \frac{K_s}{M_i}}\right) = \frac{\sqrt{\frac{M_i}{K_s}}\, z\sin\sqrt{\frac{K_s}{M_i}}\, T}{z^2 - 2z\cos\sqrt{\frac{K_s}{M_i}}\, T + 1} \tag{7-41}$$

$$\mathcal{Z}\left(\frac{1}{s(s^2 + \frac{K_s}{M_i})}\right) = \frac{M_i}{K_s}\left(\frac{z}{z-1} - \frac{z(z - \cos\sqrt{K_s/M_i}\, T)}{z^2 - 2z\cos\sqrt{K_s/M_i}\, T + 1}\right) \tag{7-42}$$

Substitution of the last two equations into Eq. (7-40) and simplifying, we have

$$z^2 + \left(\frac{K_r}{\sqrt{M_i K_s}}\sin\sqrt{\frac{K_s}{M_i}}\, T - \frac{K_p}{K_s}\cos\sqrt{\frac{K_s}{M_i}}\, T + \frac{K_p}{K_s} - 2\cos\sqrt{\frac{K_s}{M_i}}\, T\right)z + 1 + \frac{K_p}{K_s} - \frac{K_p}{K_s}\cos\sqrt{\frac{K_s}{M_i}}\, T$$

$$- \frac{K_r}{\sqrt{M_i K_s}}\sin\sqrt{\frac{K_s}{M_i}}\, T = 0 \tag{7-43}$$

Substituting the system parameters into the last equation, yielding,

$$z^2 + (14.5597\sin 0.02415T - 110.1688\cos 0.02415T + 108.1688)z + 1 - 14.5597\sin 0.02415T$$
$$-108.1688\cos 0.02415T + 108.1688 = 0 \tag{7-44}$$

The roots of the last equation as a function of T are tabulated below and the root locus diagram with T as a variable parameter is shown in Fig. 7-9. The critical value of T for asymptotic stability is approximately 5.7 sec.

Sampling period T (sec)	Characteristic Equation	Roots
0.1	$z^2 - 1.96z + 0.965 = 0$	$0.98 \pm j0.069$
0.5	$z^2 - 1.816z + 0.832 = 0$	$0.908 \pm j0.0864$
1.0	$z^2 - 1.6163z + 0.680 = 0$	$0.808 \pm j0.164$
2.0	$z^2 - 1.1686z + 0.4232 = 0$	$0.584 \pm j0.286$
3.0	$z^2 - 0.657z + 0.2298 = 0$	$0.328 \pm j0.349$

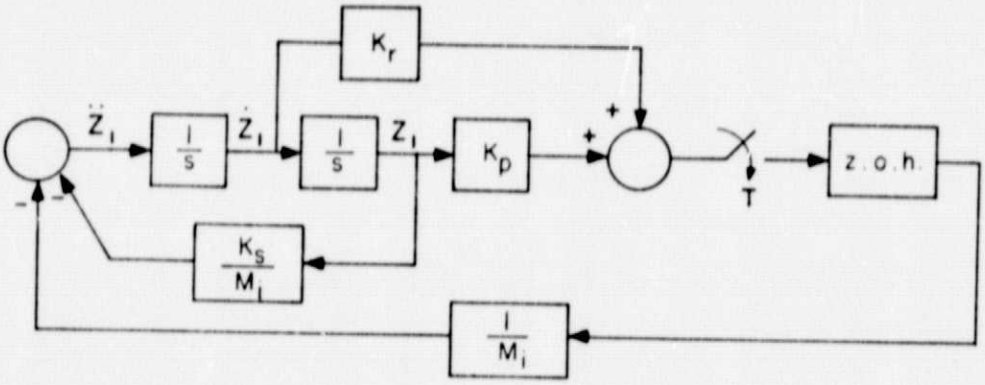

Figure 7-8. Block diagram of the linear digital ASPS payload z_1 dynamics).

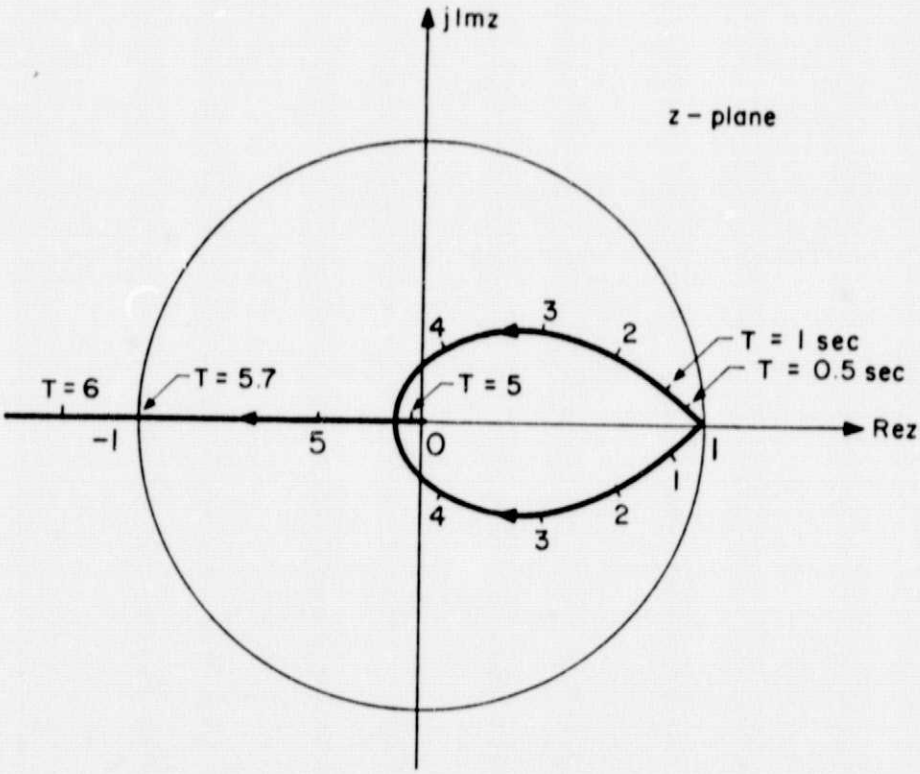

Figure 7-9. Root loci of z_1 dynamics of the digital ASPS payload as the sampling period T varies.

4.0	$z^2 - 0.0821z + 0.1 = 0$	$0.041 \pm j\,0.3135$
5.0	$z^2 + 0.556z + 0.0338 = 0$	$-0.4865,\ -0.0695$
5.7	$z^2 + 1.04z + 0.02533 = 0$	$-1.01,\ -0.025$
6.0	$z^2 + 1.257z + 0.03124 = 0$	$-1.23,\ -0.0254$

The time responses of the digital system in Fig. 7-8 for various sampling periods are shown in Fig. 7-10. The initial value of $z_1(t)$ is chosen to be 0.002 m, since the static bearing gap of z_1 is only 0.0076 m, so that the maximum constraints on the magnitude of z_1 are ± 0.0038 m. The time responses in Fig. 7-10 substantiates the root locus findings; when T = 6 sec, the closed-loop system is unstable. The time responses are quite good for T less than or equal to 3 seconds.

Effects of Quantization

The block diagram of the digital ASPS payload z_1 dynamics with the quantization effect is shown in Fig. 7-11. The input-output characteristics of the quantizer are illustrated in Fig. 7-12. The quantization level is denoted by h in meter.

The effects of quantization can be classified into three catagories: (1) stable system with steady-state error, (2) unstable system with sustained oscillation, and (3) unstable system with unbounded responses. The last case is possible since no saturation is assumed in the system model.

The steady-state error due to quatization can be determined by using the least-upper bound method [3] and the condition of sustained oscillations is found by use of the discrete describing function.

The "characteristic equation" of the system shown in Fig. 7-11 is written as

$$\Delta(z) = 1 + Q(z)(1 - z^{-1})\mathcal{Z}_0\left(\frac{1}{M_i s^2}\,\frac{K_r + K_p/s}{1 + \frac{K_s}{M_i}\,s^{-2}}\right) = 0 \qquad (7\text{-}45)$$

where Q(z) denotes the discrete describing function of the quantizer.

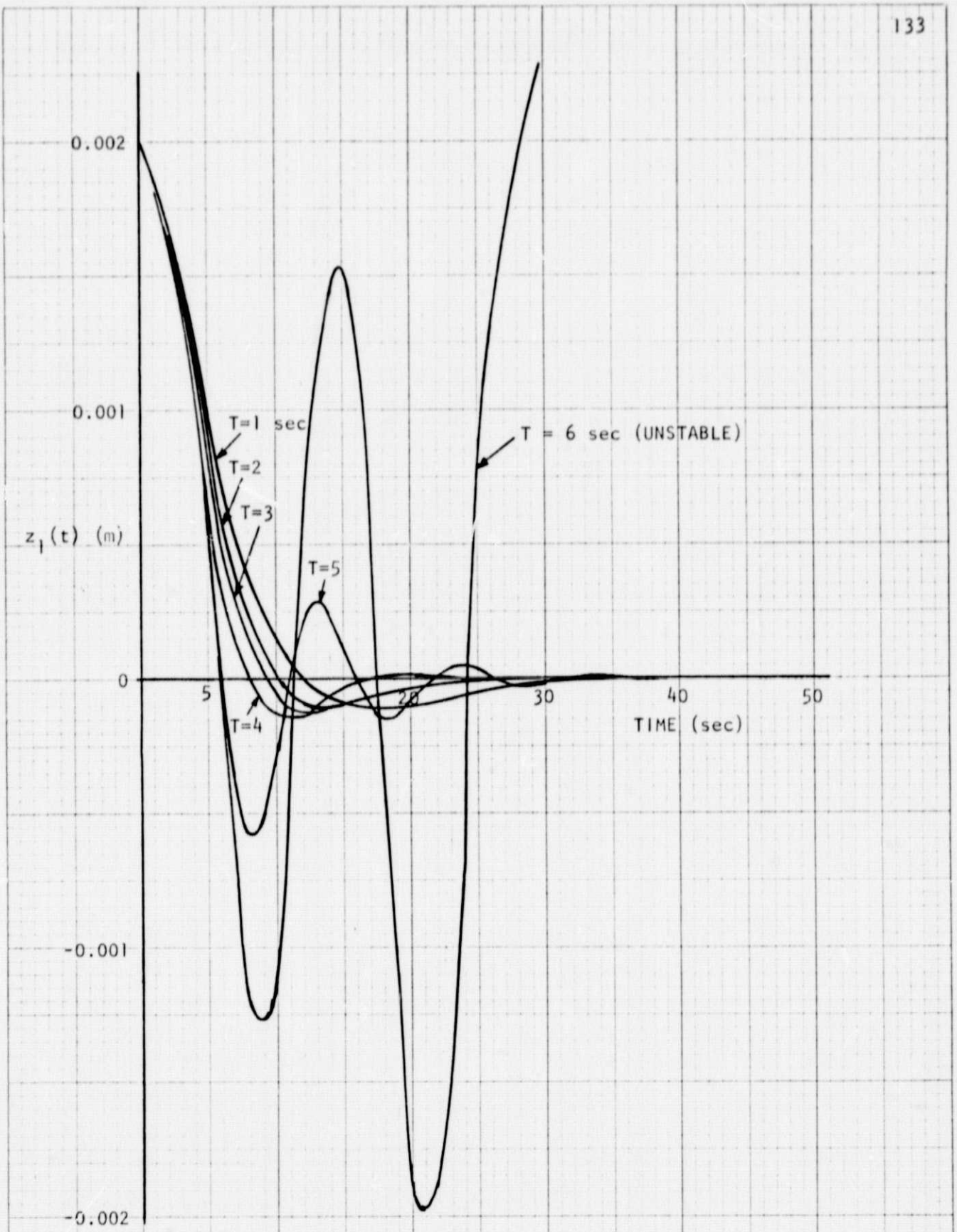

Figure 7-10. Time responses of the linear digital ASPS payload z_1 dynamics. The initial condition of z_1 is 0.002 m.

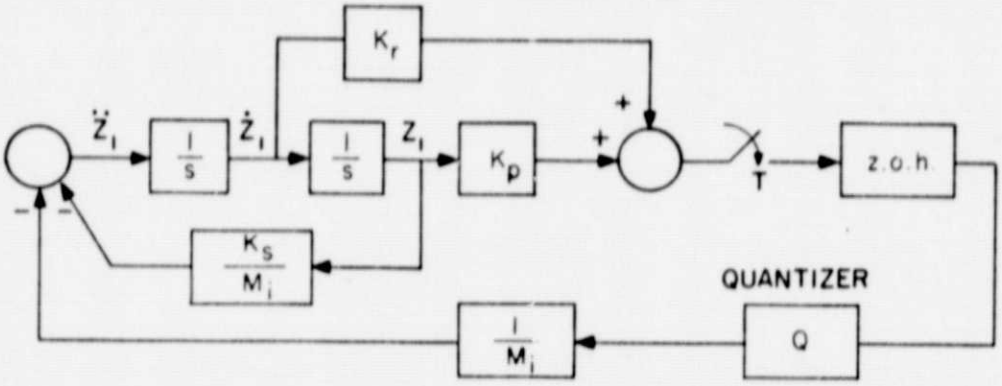

Figure 7-11. Block diagram of the digital ASPS payload z_1 dynamics with quantization.

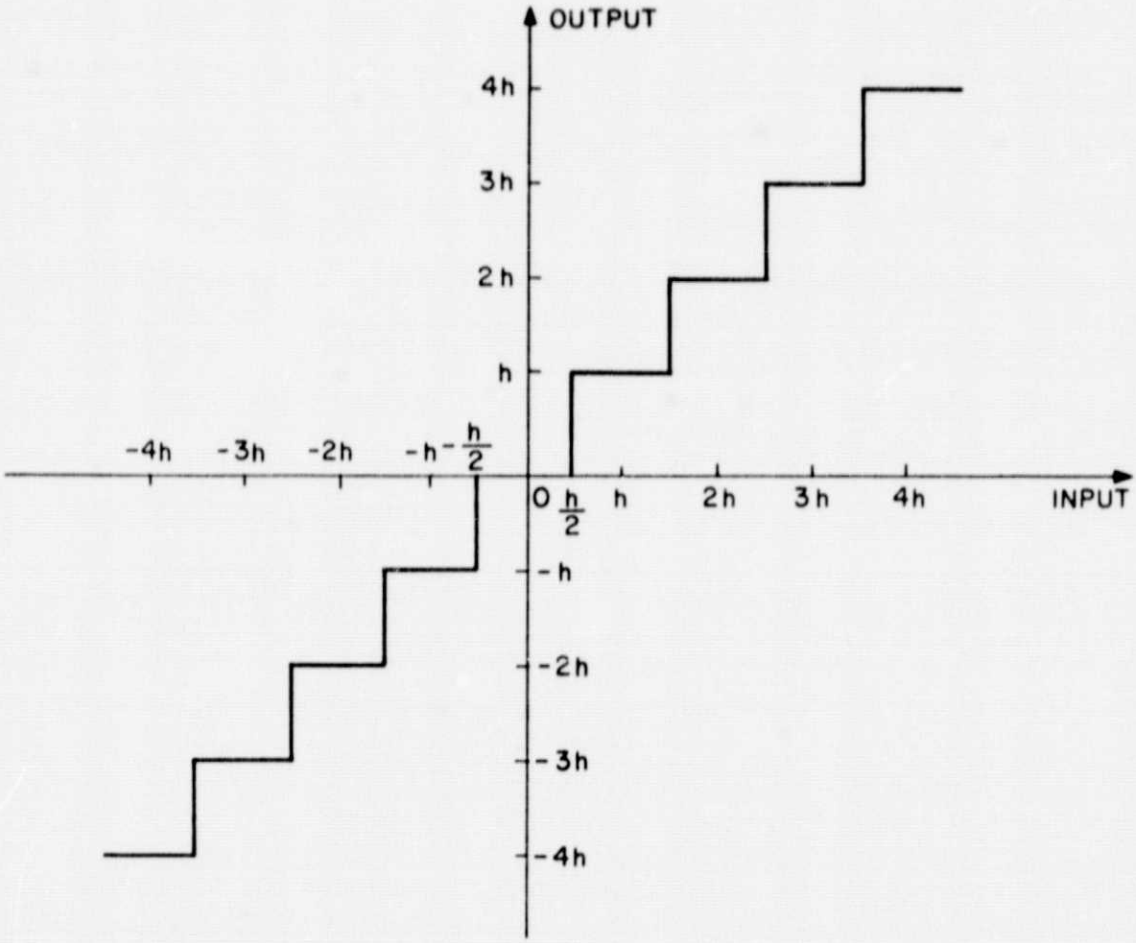

Figure 7-12. Input-output characteristics of a quantizer.

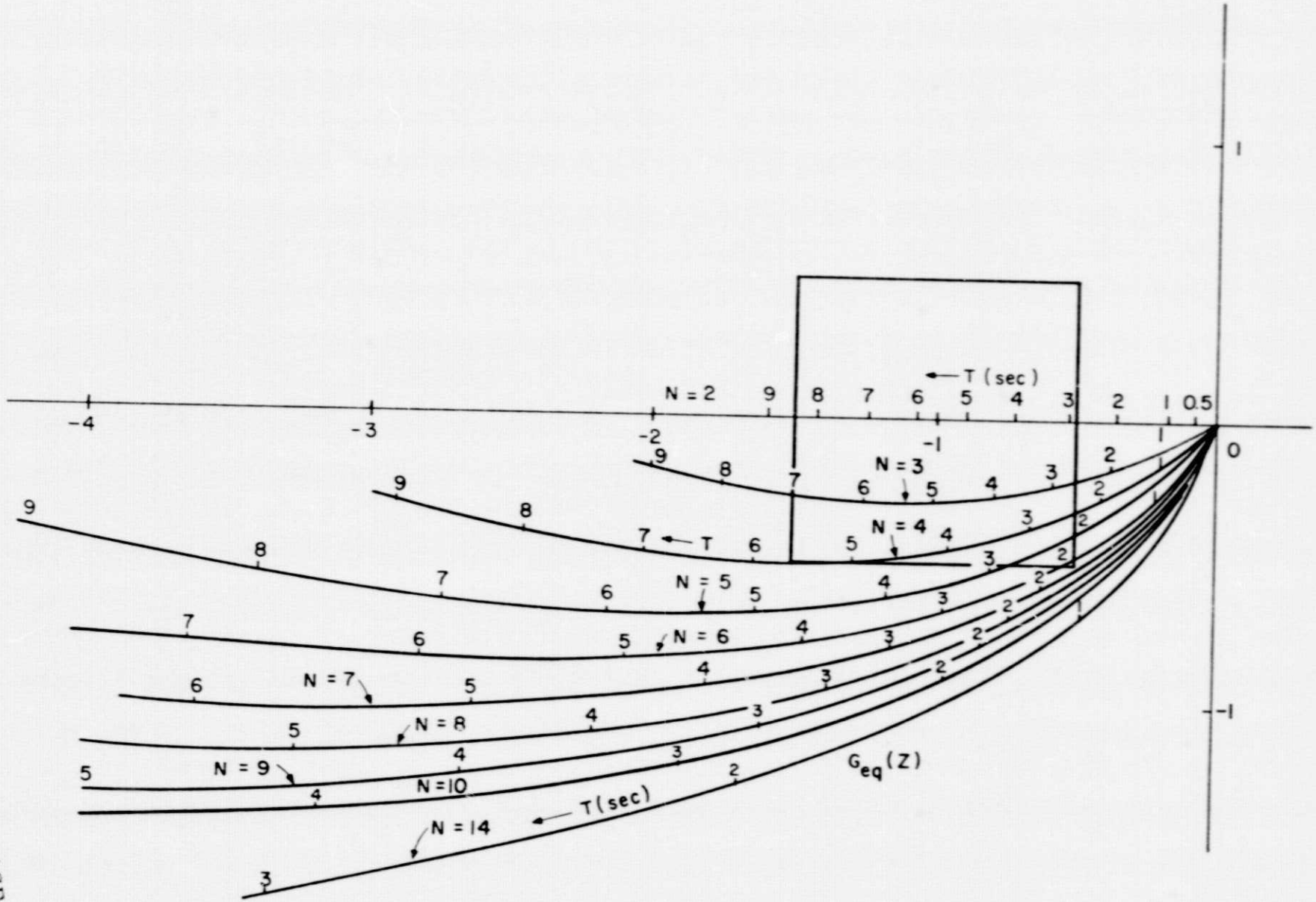

Figure 7-13. $G_{eq}(z)$ plots and critical region bounds of quantizer discrete describing function of ASPS payload z_1 dynamics; K_s = 0.35 N/m.

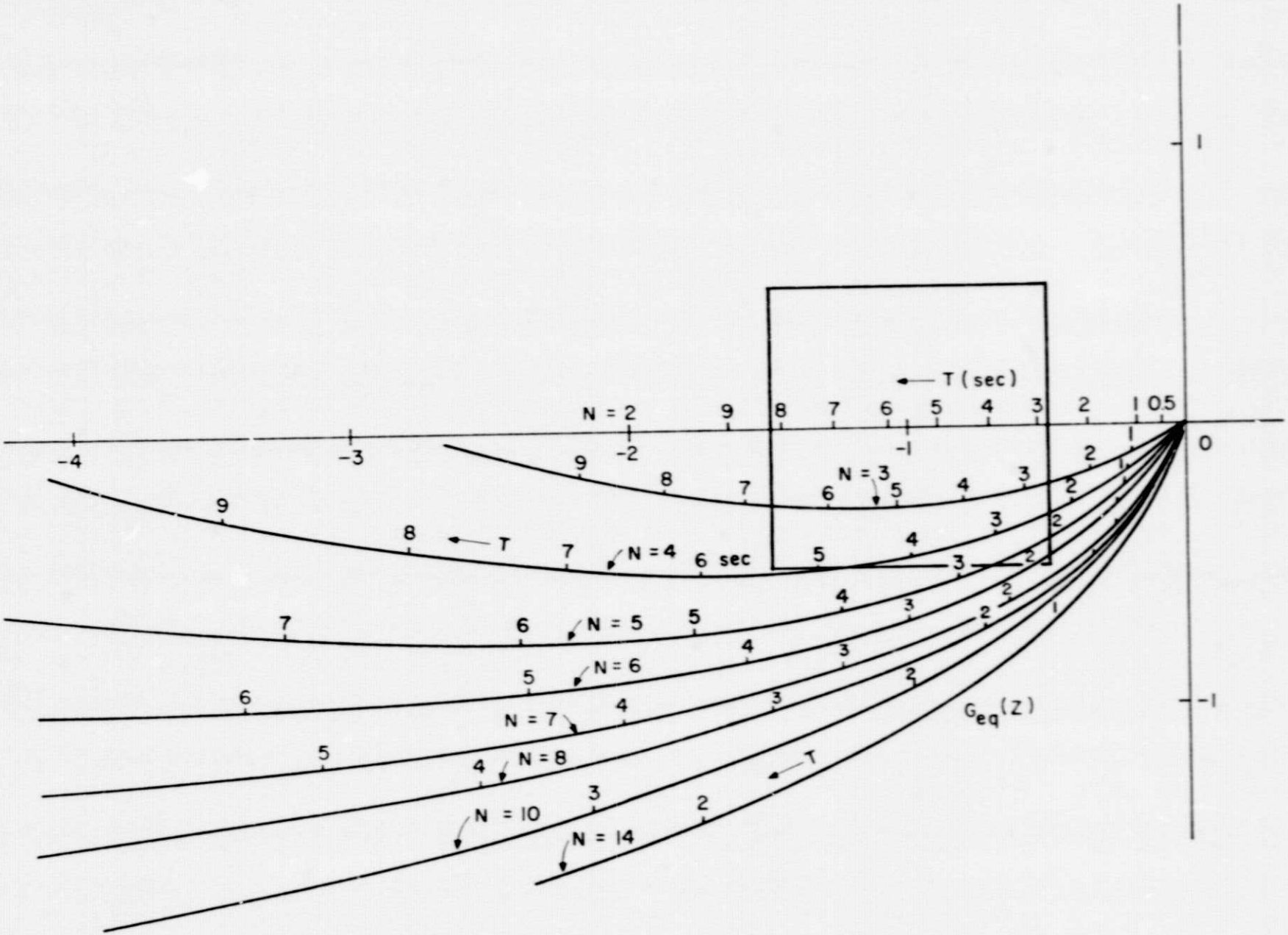

Figure 7-14. $G_{eq}(z)$ plots and critical region bounds of quantizer discrete describing function of ASPS payload z_1 dynamics; K_s = 3.5 N/m.

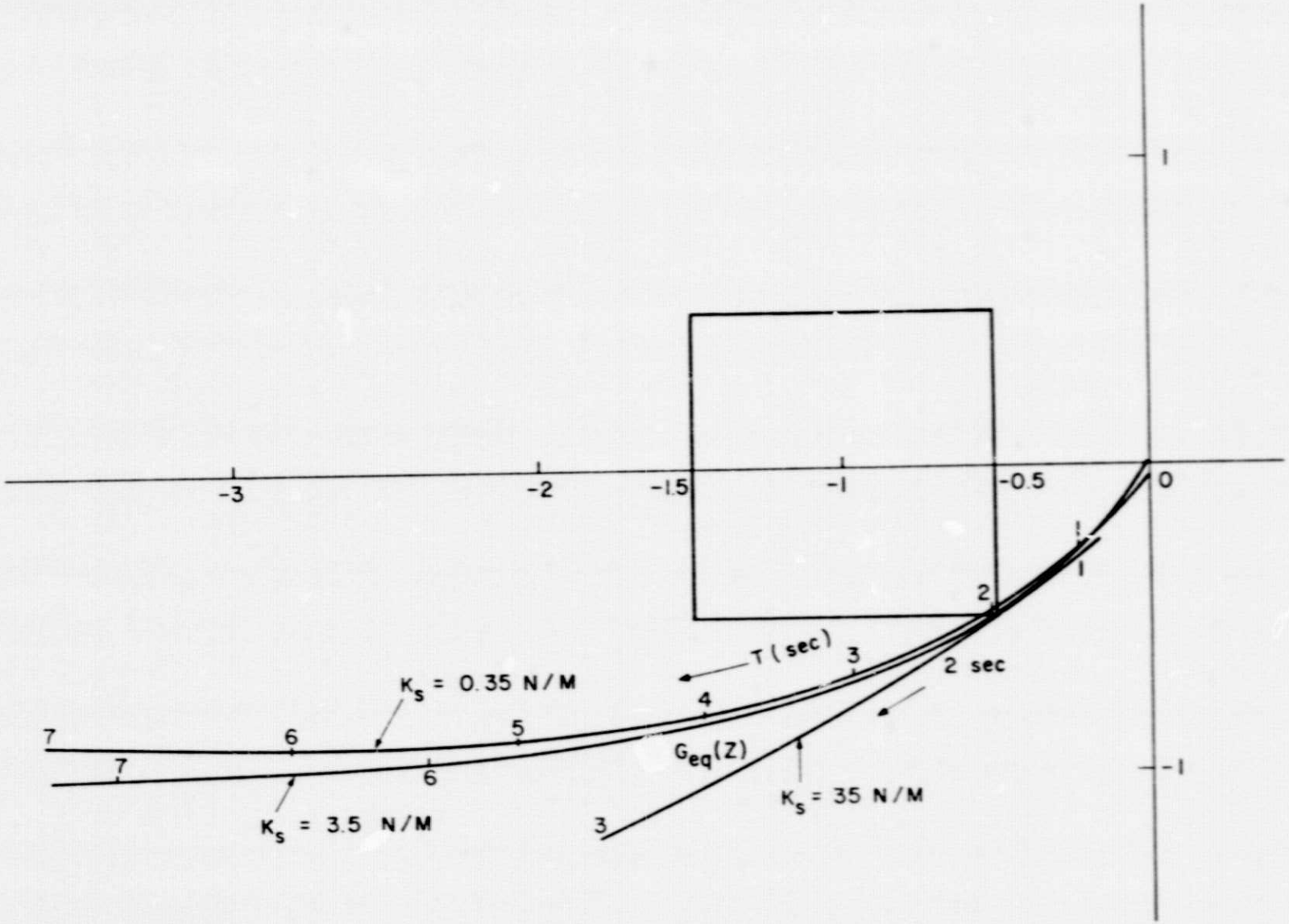

Figure 7-15. $G_{eq}(z)$ plots for N = 6 and K_s = 0.35, 3.5 and 35 N/m and critical region bounds of quantizer discrete describing function of ASPS payload z_1 dynamics.

The z-transform of the last equation is evaluated using the results in Eqs. (7-41) and (7-42). Equation (7-45) becomes

$$\Delta(z) = 1 + Q(z)G_{eq}(z) = 0 \tag{7-46}$$

where

$$G_{eq}(z) = \frac{\left(\frac{K_r}{\sqrt{M_i K_s}} \sin\sqrt{\frac{K_s}{M_i}}\,T - \frac{K_p}{K_s}\cos\sqrt{\frac{K_s}{M_i}}\,T + \frac{K_p}{K_s}\right)z - \frac{K_r}{\sqrt{M_i K_s}} \sin\sqrt{\frac{K_s}{M_i}}\,T - \frac{K_p}{K_s}\cos\sqrt{\frac{K_s}{M_i}}\,T + \frac{K_p}{K_s}}{z^2 - 2z\cos\sqrt{\frac{K_s}{M_i}}\,T + 1} \tag{7-47}$$

For $K_p = 37.861$, $K_r = 211.01$, $M_i = 600$, and $K_s = 0.35$, the last equation is simplified to

$$G_{eq}(z) = \frac{14.5597\sin 0.02415T - 108.1688\cos 0.02415T + 108.1688)z - 14.5597\sin 0.02415T - 108.1688\cos 0.02415T + 108.1688}{z^2 - 2z\cos 0.02415T + 1} \tag{7-48}$$

Figure 7-13 shows the plots of $G_{eq}(z)$ for various periods of sustained oscillations $T_c = NT$, $N = 2,3,4,\ldots$. The sampling period T varies along the curves. The square block in the figure which is centered at -1 represents the bounds on the critical regions of $-1/Q(z)$ [4] . Theoretically, the intersects between the critical regions of $-1/Q(z)$ and $G_{eq}(z)$ represent conditions of self-sustained oscillations. It is clear from Fig. 7-13 that the system should be free from sustained oscillations for all sampling periods less than 2 seconds.

Figure 7-14 illustrates the $G_{eq}(z)$ plots for $K_s = 3.5$ N/m, 10 times the nominal value. As pointed out earlier, since the mass of the payload is so large, the light spring effect of the wire cable does not materially affect the performance of the system. Figure 7-15 further illustrates that even with $K_s = 35$ N/m, 100 times the nominal value, the characteristics of the system for sampling periods less than 2 seconds are not significantly affected.

The least-upper bound error analysis of the quantization effect is performed by referring to the system block diagram shown in Fig. 7-16. The quantizer is

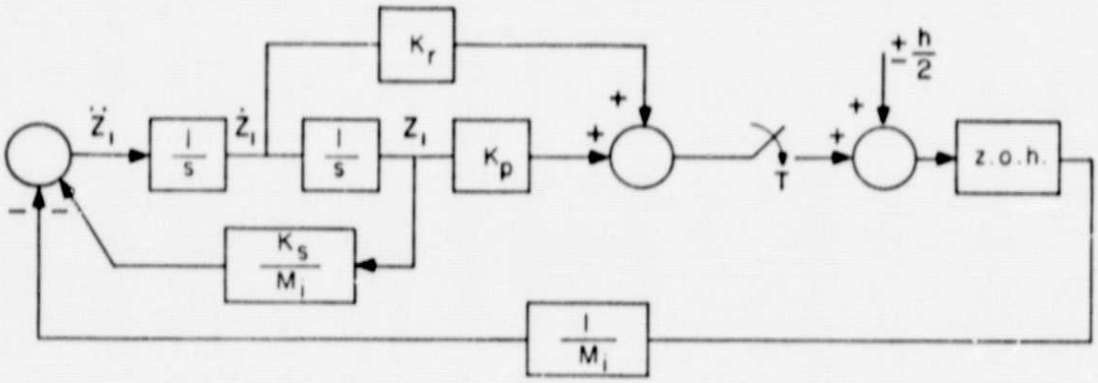

Figure 7-16. Block diagram of the digital ASPS payload z_1 dynamics for the least-upper bound analysis of quantization effects.

```
      DIMENSION FRMT(5),Y(2),DERY(2),AUX(8,2)
      EXTERNAL FCT,OUTP
      COMMON Z,ZDOT,T,AKSMI,AMINV,V1,TPRT,TEND,PRTIME,V1S,V1H
      COMMON AMI,AKS,AKP,AKR,TSP,H,AV1H,IV1H,V1HO
C
C     ALL TIME INPUTS SHOULD BE INTEGRAL MULTIPLES OF TINT.
C
      H=2.**-4
      TSP=1.
      TEND=400.
      TPRT=0.5
      TINT=0.5E-3
      Z0=0.002
      ZDOT0=0.
      ERROR=1.E-5
      AMI=600.
      AKS=0.35
      AKP=37.861
      AKR=211.01
      AKSMI=AKS/AMI
      AMINV=1./AMI
      T=0.
```

Figure 7-17. Computer program of the simulation of the ASPS payload z_1 dynamics with quantization.

```
      PRTIME=-TPRT
      PRMT(1)=T
      PRMT(2)=TEND
      PRMT(3)=TINT
      PRMT(4)=ERROR
      DERY(1)=0.5
      DERY(2)=0.5
      NDIM=2
      Y(1)=Z0
      Y(2)=ZDOT0
      CALL RKGS(PRMT,Y,DERY,NDIM,IHLF,FCT,OUTP,AUX)
      END
      SUBROUTINE FCT(TIME,Y,DERY)
      DIMENSION Y(2),DERY(2)
      COMMON Z,ZDOT,T,AKSMI,AMINV,V1,TPRT,TEND,PRTIME,V1S,V1H
      COMMON AMI,AKS,AKP,AKR,TSP,H,AV1H,IV1H,V1H0
      Z=Y(1)
      ZDOT=Y(2)
      V1=AKP*Z+AKR*ZDOT
      IF(TIME-T)40,50,50
50    T=T+TSP
      V1S=V1
40    V1H=V1S
      IF(V1H.LT.0)GO TO 20
      AV1H=(V1H/H)+0.5
      GO TO 30
20    AV1H=(V1H/H)-0.5
30    CONTINUE
      IV1H=IFIX(AV1H)
      V1H0=FLOAT(IV1H)*H
      Z2DOT=-AKSMI*Z-AMINV*V1H0
      DERY(1)=ZDOT
      DERY(2)=Z2DOT
      RETURN
      END
      SUBROUTINE OUTP(TIME,Y,DERY,IHLF,NDIM,PRMT)
      DIMENSION Y(2),DERY(2),PRMT(5)
      COMMON Z,ZDOT,T,AKSMI,AMINV,V1,TPRT,TEND,PRTIME,V1S,V1H
      COMMON AMI,AKS,AKP,AKR,TSP,H,AV1H,IV1H,V1H0
      IF((TIME-PRTIME).LT.TPRT)RETURN
      PRTIME=PRTIME+TPRT
      WRITE(5,100) TIME,V1,V1H,V1H0,(Y(I),I=1,2),IHLF
100   FORMAT(1X,F5.2,1X,E12.5,1X,E12.5,1X,E12.5,1X,2(1X,E12.5),1X,I2)
      RETURN
      END
```

Figure 7-17. Computer program of the simulation of the ASPS payload z_1 dynamics with quantization.

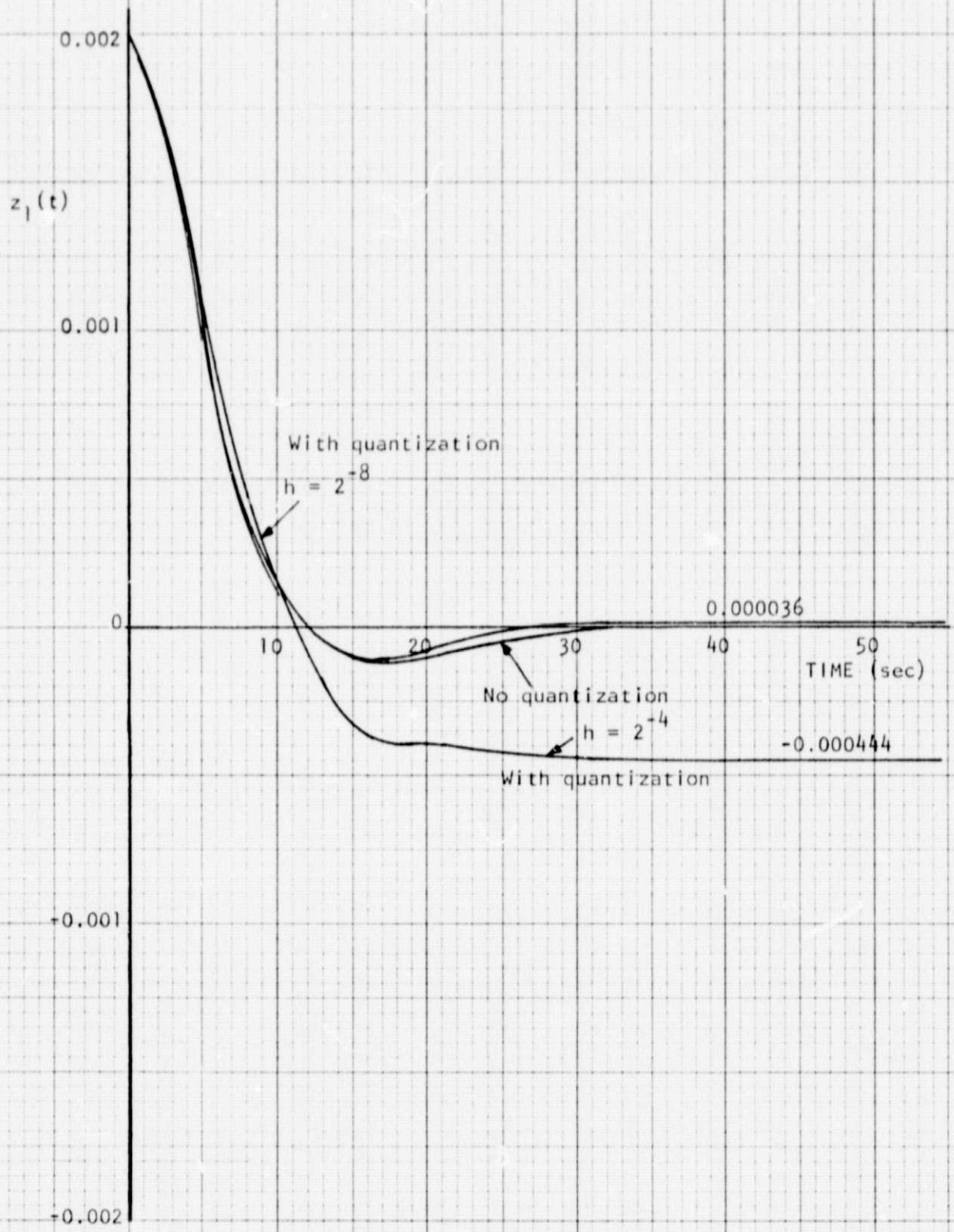

Figure 7-18. Time responses of the digital ASPS payload z_1 dynamics; with and without quantization. T = 1 second.

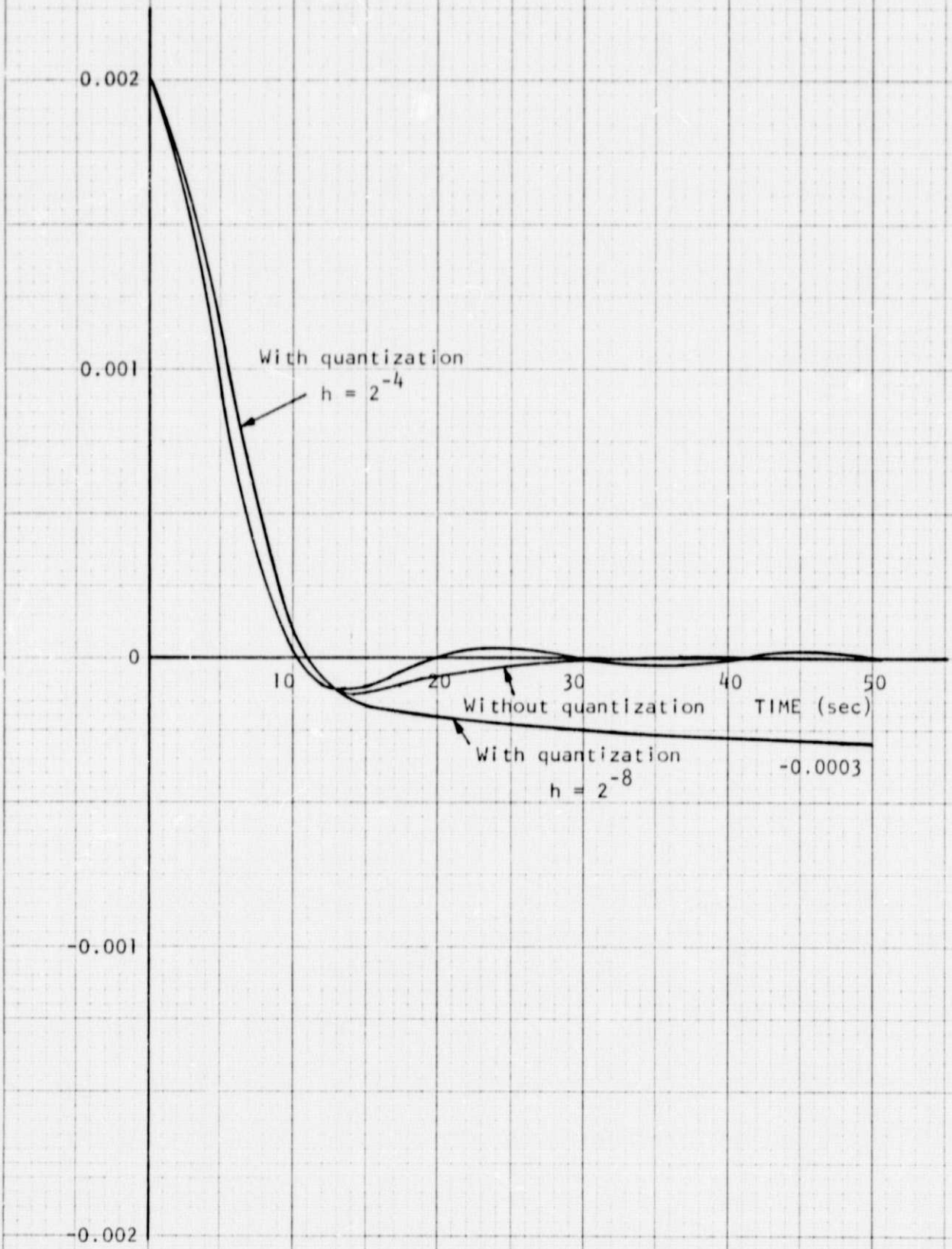

Figure 7-19. Time responses of the digital ASPS payload z_1 dynamics; with and without quantization. T = 2 seconds.

replaced by the noise input with an amplitude of $\pm h/2$.

The z-transform of the displacement z_1 due to the noise input is

$$Z_1(z) = \frac{(1 - z^{-1})}{\Delta(z)} \mathcal{Z}\left(\frac{1}{M_i s^3(1 + K_s s^{-2}/M_i)}\right)(\pm h/2)\frac{z}{z - 1} \tag{7-49}$$

where $\Delta(z)$ is as given in Eq. (7-40).

In Eq. (7-49),

$$(1 - z^{-1})\mathcal{Z}\left(\frac{1}{M_i s^3(1 + K_s s^{-2}/M_i)}\right) = (1 - z^{-1})\mathcal{Z}\left(\frac{1}{M_i s(s^2 + K_s/M_i)}\right)$$

$$= \frac{1}{K_s}\frac{(z + 1)(1 - \cos\sqrt{K_s/M_i}\,T)}{z^2 - 2z\cos\sqrt{K_s/M_i}\,T + 1} \tag{7-50}$$

Thus,

$$Z_1(z) = \frac{\frac{1}{K_s}(z + 1)(1 - \cos\sqrt{K_s/M_i}\,T)(\pm\frac{h}{2})(\frac{z}{z - 1})}{z^2 + \left(\frac{K_r}{\sqrt{M_i K_s}}\sin\sqrt{\frac{K_s}{M_i}}\,T - \frac{K_p}{K_s}\cos\sqrt{\frac{K_s}{M_i}}\,T + \frac{K_p}{K_s} - 2\cos\sqrt{\frac{K_s}{M_i}}\,T\right)z + 1 + \frac{K_p}{K_s} - \frac{K_p}{K_s}\cos\sqrt{\frac{K_s}{M_i}}\,T - \frac{K_r}{M_i K_s}\sin\sqrt{\frac{K_s}{M_i}}\,T} \tag{7-51}$$

The final steady-state value of $z_1(kT)$ is given by

$$\lim_{k\to\infty} z_1(kT) = \lim_{z=1}(1 - z^{-1})$$

$$= \frac{\frac{2}{K_s}(1 - \cos\frac{K_s}{M_i}T)(\pm\frac{h}{2})}{2(1 + \frac{K_p}{K_s})(1 - \cos\frac{K_s}{M_i}T)} = \frac{\pm\frac{h}{2}}{K_s + K_p} \tag{7-52}$$

This result shows that the least-upper bound on the steady-state value of $z_1(kT)$ due to quantization is inversely proportional to K_s and K_p.

For the given values of K_s and K_p, we have

$$\lim_{k\to\infty} z_1(kT) = \frac{\pm \frac{h}{2}}{38.211} = \pm\, 0.013085237h \qquad (7\text{-}53)$$

Thus, for a quantization level of 2^{-4}, the final error in z_1 is ± 0.000817827 m, whereas it is ± 0.000051114 m for a quantization level of 2^{-8}.

7.4 Computer Simulation of the ASPS Payload z_1 Dynamics with Quantization

In this section the z_1 dynamics of the ASPS payload are simulated to study the effects of quantization. The computer program is given in Fig. 7-17.

Figure 7-18 illustrates the time responses of $z_1(t)$ of the ASPS payload with and without quantization, for the sampling period of T = 1 second. The initial value of $z_1(t)$ was chosen to be 0.002 m. As predicted by the discrete describing function analysis, the system does not exhibit any sustained oscillations when T = 1 sec. However, the nonzero quantization levels did produce steady-state errors in $z_1(t)$. The computer simulated results and the results obtained by the least-upper bound method are tabuiated below for comparison. It is expected that the errors predicted by the least-upper bound method will be greater, since it is a worst-case study.

Sampling Period T = 1 sec

Quantization level h (m)	$z_1(\infty)$ least-upper bound (m)	$z_1(\infty)$ simulation (m)
2^{-4}	$\pm$ 0.0008178	-0.000444
2^{-8}	$\pm$ 0.000051114	0.000036

Figure 7-18 also shows that with the quantization level of 2^{-8} (8 bits), the time response of $z_1(t)$ is very close to that of $z_1(t)$ without quantization, so that a larger word length seems unnecessary unless a smaller steady-state error is required.

Figure 7-19 illustrates the time responses of $z_1(t)$ for T = 2 sec. For $h = 2^{-4}$, the error is -0.0003 at t = 50 sec and still increasing. For $h = 2^{-8}$,

the response actually exhibited a sustained oscillation with a peak-to-peak amplitude of 0.000066 m. As shown in Fig. 7-13, when T = 2 sec, the system is marginal in generating sustained oscillations. It should be noted that the digital computer is not the most suitable for simulating digital systems with quantizers, since the computer itself is a digital system with its own quantization levels. However, the results obtained here are conclusive enough to indicate the quantization effects in the ASPS payload, and are useful in the selection of the sampling period and the quantization level.

For sampling periods greater than 2 seconds, the computer simulation results showed that sustained oscillations always existed.

References

1. Technical Report, Space Shuttle Experiment Pointing Mount (EPM) Systems, An Evaluation of Concepts and Technologies, Jet Propulsion Laboratory 701-1, April 1, 1977.
2. H. B. Waites, Equations of Motion Derivation for a Simplified ASPS Model, Memorandum, NASA, October 1977.
3. B. C. Kuo, DIGITAL CONTROL SYSTEMS, SRL Publishing Company, 1977.
4. Final Report, Stability Analysis of the Low-Cost Large Space Telescope System, Systems Research Laboratory, June 30, 1975.